ON WAVEFORM SELECTION IN A TIME VARYING SONAR ENVIRONMENT

Ashley I. Larsson[1*] and Chris Gillard[1]

(1) Maritime Operations Division, Defence Science and Technology Organisation, Edinburgh, Australia

Abstract

The best waveform to use in different scenarios has always been an issue for the Navy. Waveform choice is often based on minimising the effects of reverberation or searching for a feature of the target such as Doppler. A recent paper on environmental acoustics [1] showed that in a time varying environment, the probability distribution of received signal energy changes with the type of waveform used. In this paper we consider a similar acoustic environment with time variation and look at the effect of different waveforms on the probability of detection in an ambient noise limited environment.

Nomenclature

A	Amplitude of the source waveform
α_j	Amplitude of the arrival from ray path j
B	Bandwidth of the waveform
n	noise (White Gaussian noise)
p	Output from the source
s	Input waveform to the source
t	Time
τ_j	Time delay of arrival from ray path j
T	Duration of the waveform 1 second
u	Input vector
μ	random perturbation in time delays
υ	Correlator time delay
x	Environmentally affected waveform plus noise
y	Received waveform without noise
z	Output from the correlator receiver
ω_0	center radial frequency

Introduction

Choosing a particular waveform for an environment has been a long-term issue for active sonar operators and designers. The interest in this issue has recently increased because modern active sonar systems are capable of emitting a variety of broadband pulses.

The advice for waveform selection is normally based on reverberation considerations [2] and the mean performance of a pulse. In conditions where ambient noise limits the performance of a receiver rather than reverberation, only the mean performance is used and this is usually based on the mean transmission loss or signal to noise ratio at the centre frequency of the pulse. This measure is often converted to a probability of detection and the waveform chosen is the one that gives the highest probability of detection for a fixed false alarm rate [3] [4]. However, using this measure, any waveform with the same source level and centre frequency would have the same performance. This measure does not consider waveform type, bandwidth, or effects of multipath acoustic propagation and the temporal variability in the acoustic environment. The detection performance also depends on the processing inside the receiver. The conventional correlator receiver with detector searches the received data for a waveform that is similar in form to the one emitted. The probability of detecting such a waveform in noisy data depends on the waveform's ability to maintain its initial form while propagating through the environment. In an environment that distorts the waveform, the probability of detection will vary with the waveform chosen. In a time varying environment a variety of distortions will occur.

The shallow water environment distorts the waveform because of multipath propagation. The interference between arrivals cancels the energy at some frequencies and enhances the energy in others, thus distorting the waveform. Also wave motion of the sea surface, seafloor roughness, seaweed motion, ocean currents and sonar sensor motion introduce time variability into the interference. This time variability will add statistical fluctuations to the waveform's performance. Shallow water regions in Australian littoral environments are often time varying. Furthermore, in these regions it is also common for ambient noise to be the major factor in masking the distorted received waveform thus limiting the ability of a sonar system to detect a target.

In this paper we use acoustic simulation to investigate the performance of three different waveforms in a time-varying, ambient noise limited shallow water environment. The simulated data are pulses that have been propagated one way through the environment. Here we only consider waveform distortions caused by the environment, and ignore target scattering and nonlinear effects in the receiver. The probability of detection for each waveform is determined by propagating each waveform through a large number of time dependent environmental realizations, and calculating the number of detections made after the data has passed through a correlator receiver and a Constant False Alarm Rate (CFAR) detector. This simulation will show that the three waveforms, which have the same source level and centre frequency, have a very different probability of detection. The major causes of the probabilities changing with waveform type will also be discussed.

The Model

The simulation can be broken into components as shown in the schematic diagram of figure 1. The

components are the source, the propagation model, which models the environmental effects on the pulse, the correlator receiver, and the detector. The variables indicating the inputs and the outputs of each component are also shown in figure 1. The modeling in each component is described below.

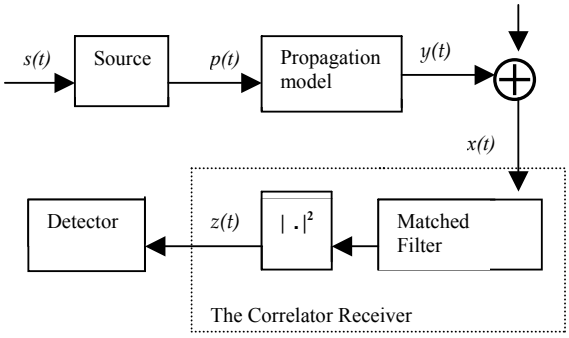

Figure 1. Schematic diagram of the system with the environment included.

The Source Model

The source amplifies the input signal *s(t)* and limits its bandwidth to 1 kHz. In the simulations, four source levels (SL) 125, 131, 134 and 137 dB, are used to compute a family of Receiver Operator Characteristic (ROC) [3] curves for each waveform. In each case, input waveforms having unit energy are amplified to obtain the appropriate source level. There were three input waveform types, each of one-second duration and with a centre frequency of 7.5 kHz, a single frequency Continuous Wave (CW) pulse, a 200 Hz bandwidth Linear Frequency Modulated (LFM) pulse and a 13 bit Barker code Binary Phase Shift Key (BPSK) pulse.

The CW pulse is a single tone burst with a 10% cosine taper on each end. The LFM pulse is of the form

$$s(t) = \sin(w_0 t + Bt^2/2), \quad (1)$$

and was tapered in the same manner as the CW pulse. The envelope of the LFM and CW pulse is shown in figure 2.

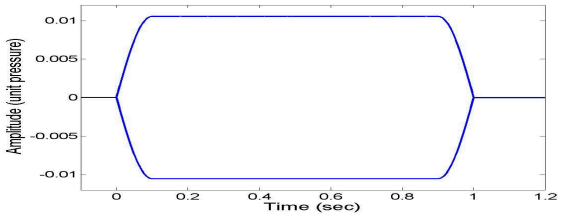

Figure 2: The envelope of the emitted LFM and CW tapered pulses

Thirteen tonal bursts abutted together make the BPSK pulse and each of these bursts were multiplied by an amplitude called a bit. The first tonal burst is multiplied by the first bit and so on. The thirteen bits for the Barker code are [1,1,1,1,1,-1,-1,1,1,-1,1,-1,1]. For more details see reference [5]. Each tonal burst in the BPSK has a 1/13 second duration making the total duration of the pulse 1 second and giving the pulse a bandwidth of approximately 13 Hz. Figure 3 shows the envelope of the BPSK. The envelope of this pulse is the envelope of the 13 tonal bursts abutted together. Where the phase changes by π between each segment, the division in the envelope is not a great.

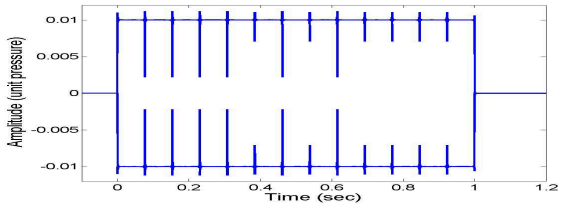

Figure 3: Envelope of the emitted BPSK pulses

The source output waveform *p(t)* is

$$p(t) = As(t). \quad (2)$$

Propagation Model

The propagation model used was Bellhop [6] [7], which uses Gaussian beam ray theory. The channel environment and the method used to compute the perturbations in the ray arrivals were the same as that described by Duncan et al. [1]. The channel was a 150 m deep iso-speed water column, with a sound speed of 1500 m/s and a density of 1024 kg/m^3. The seabed was a fluid half-space with a sound speed of 1750 m/s, a density of 1940 kg/m^3, and an attenuation of 0.8 dB per wavelength. The source and receiver were located at depths of 6 m and 10 m, respectively, and the distance between the source and receiver was 4 km, which is the only difference to the scenario in reference [1]. Figure 4 provides a physical picture of the scenario.

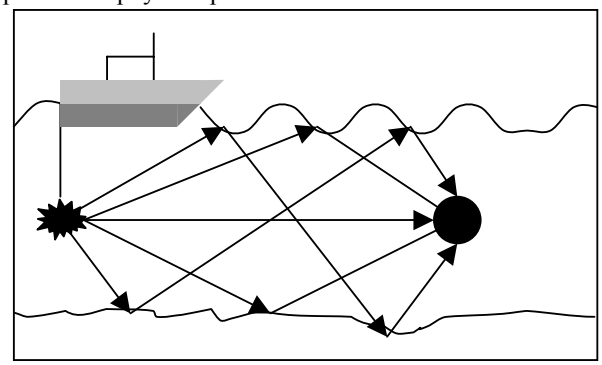

Figure 4: The physical picture of one way propagation with rays.

This figure shows straight-line rays, which exist for an iso-speed water column. The lengths of the ray paths were randomly perturbed to simulate time variation in the environment due to phenomena such as wave motion of the sea surface, the roughness of the sea floor, the motion of seaweed and the currents in the ocean.

The Bellhop model [6] [7] provided amplitudes α_j and delays τ_j of the different ray arrivals. For the environment described above, 39 rays were found to have amplitudes greater than 1% of the largest ray

amplitude. A random perturbation μ seconds was added to the delay of each ray arrival. This perturbation was different for each ray path and environmental realization. The random perturbations were generated from a Gaussian random number generator with a standard deviation of 200 μsecs, as used by Duncan et. al. [1]. The range of pulse realizations does not vary for a standard deviation greater than a quarter of a period of the lowest frequency present according to reference [1].

Each realization was calculated by summing the replicas of the transmitted waveform delayed and scaled by the amounts given by Bellhop. The output becomes

$$y(t) = \sum_{j=1}^{39} \alpha_j p(t - \tau_j - \mu). \quad (3)$$

The calculation of all the realizations of the received waveform was performed in the frequency domain to avoid interpolation errors.

Figures 5 through 7 show envelope functions for five realizations of the CW, BPSK and LFM waveforms, respectively. Notice the amplitudes for the CW waveforms vary more than the amplitudes from the other waveforms.

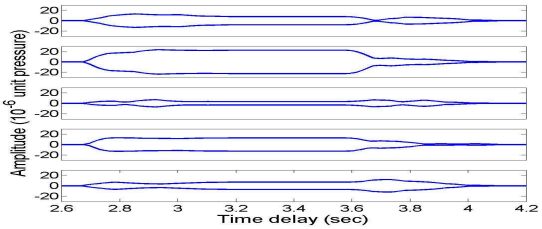

Figure 5: Envelopes of the CW waveform

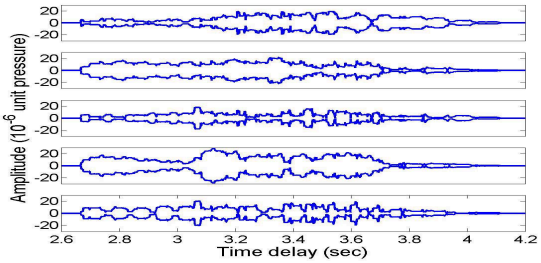

Figure 6:Envelopes of the BPSK waveform

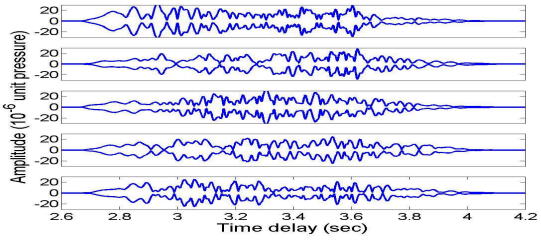

Figure 7:Envelopes of the LFM waveform

Gaussian distributed noise is added to each realisation before being processed by the correlator receiver. The standard deviation of this noise was based upon a noise level of 60 dB (re unit pressure^2/Hz). The received data is

$$x(t)=y(t)+n(t). \quad (4)$$

The distribution of energy arriving at the receiver for 1000 realisations is shown in figure 8 for each waveform. It is evident that for each waveform, the mean energy level of the arrivals is slightly different whilst the variances are very different. It will therefore be the variance in the signal to noise ratio that will cause the major differences in the performance of the waveforms.

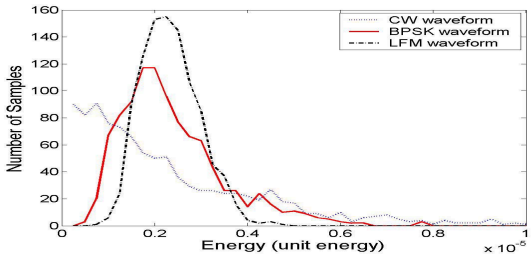

Figure 8: Histograms of the arriving energy

The Correlator Receiver

Received data, *x(t)* that have distortions modeled by the propagation model are processed in a correlator receiver using a matched filter and an absolute function squared. The output of the receiver, *z(t)* is given by

$$z(\upsilon) = \left| \int_0^T x(t-\upsilon)s^*(t)dt \right|^2 \quad (5)$$

for the continuous time domain, where * is the conjugate. Figures 9, 10 and 11 show five realizations of the receiver output for the CW, BPSK and LFM waveforms without noise (i.e., signal only), respectively, whilst figures 12, 13, and 14 show five realizations of the receiver output for ambient noise only for the CW, BPSK and LFM matched filters, respectively. The LFM receiver outputs are on a different scale to the other figures. Also notice that the maximum amplitude of the noise increases with increasing matched filter bandwidth.

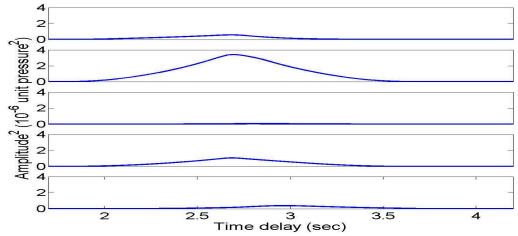

Figure 9: CW receiver outputs to the detector.

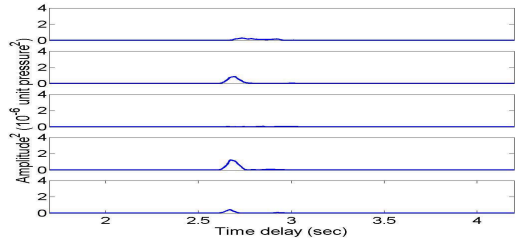

Figure 10:BPSK receiver outputs to the detector

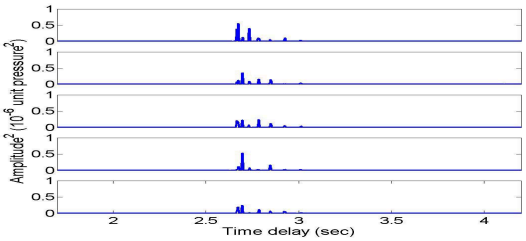

Figure 11: LFM receiver outputs to the detector (note different amplitude scale)

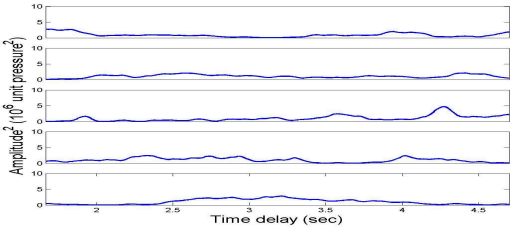

Figure 12: Amplitudes of noise passed through a CW matched filter.

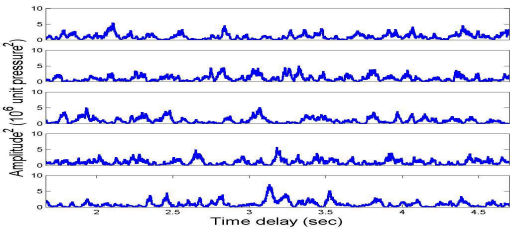

Figure 13: Amplitudes of noise passed through a BPSK matched filter

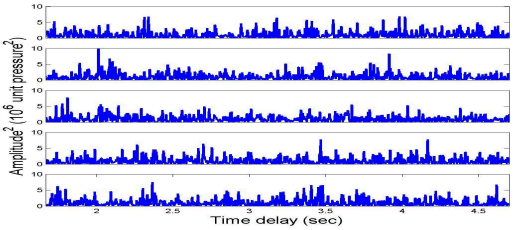

Figure 14: Amplitudes of noise passed through a LFM matched filter

Detector

The detector used for this analysis is a constant false alarm rate (CFAR) detector [8] with the threshold set according to an acceptable probability of false alarm. The detector operates by declaring a detection when the value of $z(t)$ at time t exceeds a threshold, indicating that a good replica of the sent waveform has been found at time delay t. The number of false alarms, missed detections and true detections characterize the performance of the detector. A false alarm occurs when the detector has declared a detection in the absence of the signal waveform, a missed detection occurs when the detector has declared no detection in the presence of the signal waveform, and a true detection occurs when the detector declares detection when a signal waveform is present. In an acoustic environment having only one ray path, a true detection would occur at a time t corresponding to the time when the beginning of the waveform reaches the receiver. However, the acoustic environment considered here has multiple ray paths, and the mean time difference between the first and last arrivals for the time varying environment is 0.557 seconds. Each arrival can be the cause of a true detection. Therefore assuming a signal waveform with time resolution equal to $1/B$, true detection in the multipath environment occurs if detection is declared in the time period between the first ray arrival minus $1/B$, and the last ray arrival plus $1/B$. We call this time period the detection time window. In this analysis, the detection time window was computed using the mean rather than the actual arrival time differences, because time variations in the ray arrivals due to environmental variation are small compared to the difference in arrival times.

Performance of Waveforms

The best waveform to choose for sonar target detection is one that gives a high probability of detection for a fixed probability of false alarm. Receiver Operating Characteristic (ROC) curves [3] are often used to represent the detection performance of different detection schemes as a function of SNR. However, time variations in the acoustic environment will cause the SNR for each pulse to vary from one realization to the next, making it difficult to simulate the detection performance at a constant SNR. To overcome this problem the ROC curves for each waveform are computed for each of the four source levels considered, assuming a constant noise spectral density of 60dB (re unit pressure^2/Hz) at the input to the correlator receiver as discussed previously. However, as a guide, the CW waveform with a source level of 125 dB has a mean SNR of 8.806 dB at the receiver.

Calculating the ROC curves

ROC curves were computed using 21 probabilities of false alarm equally spaced on a log scale from 10^{-2} to 10^{-6}. From these probabilities, 21 corresponding detection thresholds were calculated based on the distribution of the noise samples at the input to the detector. To collect these samples, one thousand realizations of white Gaussian noise sequences, 3.28 seconds long (2^{16} samples at a sampling rate of 20 kHz) were generated. These realisations were then passed through the appropriate matched filter (i.e. CW, BPSK, or LFM) and the maximum amplitude of the correlated noise within the detection time window was stored as a noise sample. To maintain consistent statistics, the probability of detection and probability of false alarm were calculated using simulation data from the same detection time windows.

Histograms for the maximum matched filtered noise samples are shown in figure 15 and the calculated thresholds are shown in figure 16. When calculating the thresholds for low probabilities of false alarm, the histograms had to be extrapolated using exponential

curves because there were insufficient samples for integration. An exponential fit was used because the distribution of the matched filtered noise is Gaussian and its amplitude square is chi-squared distributed, which has an exponential tail. The maximum of the matched filtered data is an ordered statistic and [9] shows the distribution of a maximum as being a function of the cumulative distribution function, which is near 1 at the tail, multiplied by the probability density function of the initial data. Thus the distribution of the tail is expected to be exponential and an exponential fit can be applied.

Next we compute probabilities of detection by applying the thresholds to histograms of simulated true detection samples. These true detection samples are the maximum amplitude in the detection time window of the receiver output produced from a signal plus noise realization. For consistency, the noise added to each signal realization is one of the sequences of noise used to compute the detection thresholds. Histograms of true detection samples computed from 1000 realisations of the time-varying environment are shown in figures 17, 18 and 19 for the CW, BPSK and LFM waveforms respectively. The probability of detection is then the fraction of true detection samples that occur above the threshold. Computed ROC curves at four different source levels for the CW, BPSK and LFM waveforms are shown in figure 20, 21and 22 respectively.

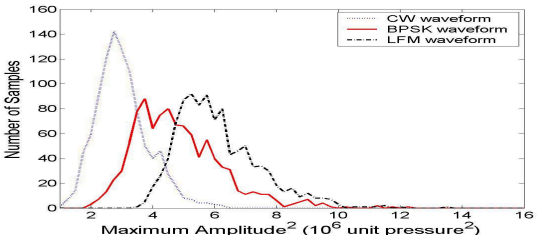

Figure 15: Histograms of the maximum matched filtered amplitudes of noise

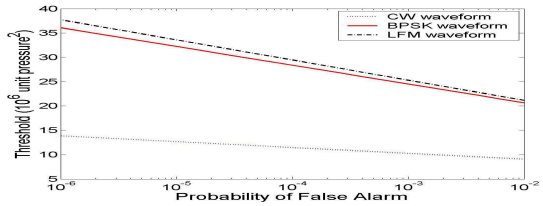

Figure 16: Thresholds against probability of false alarm for the three waveforms

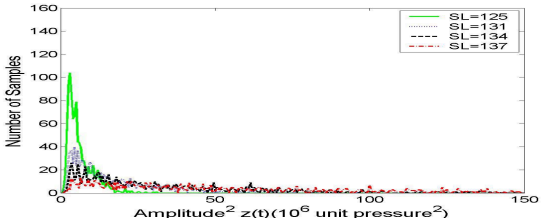

Figure 17: Histogram of the maximum amplitudes for the CW pulse

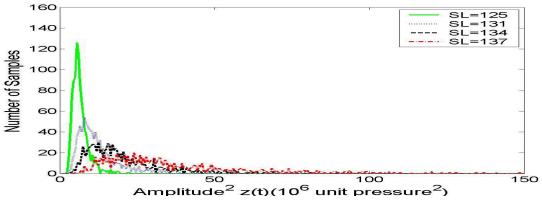

Figure 18: Histogram of the maximum amplitudes for the BPSK pulse

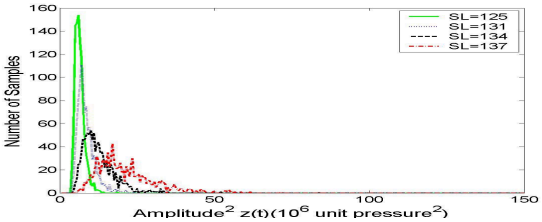

Figure 19: Histogram of the maximum amplitudes for the LFM pulse.

Discussion

The performance of each waveform is significantly different. Figure 23 highlights this difference by displaying the ROC curves of the three waveforms for a source level of 137 dB. This figure shows the CW waveform gave the best performance and the 200 Hz LFM the worst

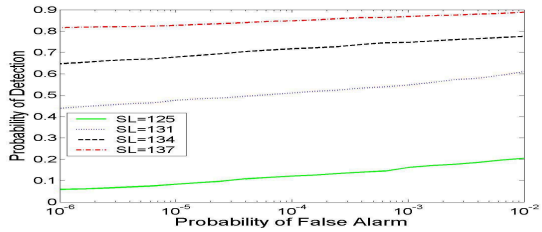

Figure 20: ROC curves for the CW pulse

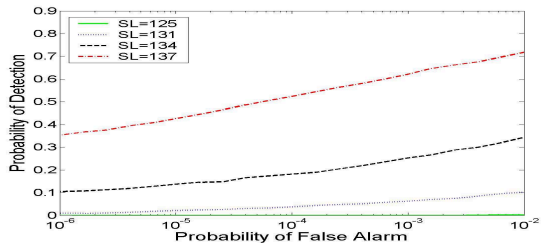

Figure 21: ROC curves for the BPSK pulse

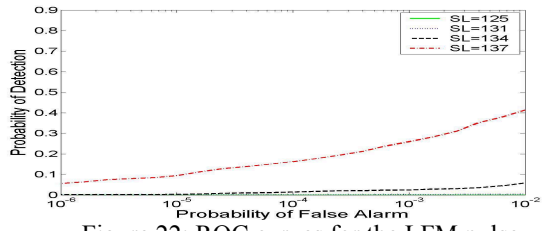

Figure 22: ROC curves for the LFM pulse

The CW gave the best performance for two reasons. The first and most significant reason is the CW has the greatest range of arrival energy, (as seen in Figure 8) and therefore has more realisations with arrival energies above the high threshold required to achieve low

probabilities of false alarm. The CW waveform will always have a greater range of arrival energy because each environmental realisation has a dramatic effect on the transmission loss at a single frequency. In contrast, the energy loss for broadband waveforms is a weighted average transmission loss of the individual frequencies in the waveform.

The second reason is the setting of the threshold. The distribution of the noise is affected by the matched filtering, and the noise processed through a CW matched filter produces the lowest maximum noise amplitudes, resulting in a lower threshold compared to the other waveforms (see figure 16).

The variance in arrival energy and the change in distribution of the matched filtered noise affects the probability of detection as shown in figure 23. The results show that the CW waveform has a probability of detection of 0.82 at a probability of false alarm of 10^{-6} whilst the LFM has a probability of detection of 0.08 at the same probability of false alarm. These effects cannot be predicted using the mean signal to noise ratio.

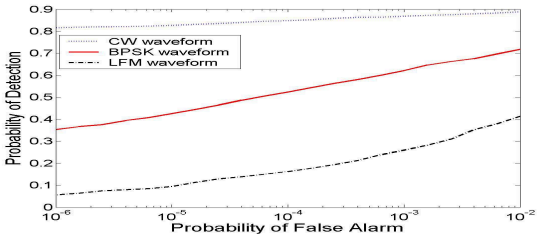

Figure 23: Comparison of the ROC curves from different pulses for the 137 dB source level

Conclusions

This paper shows the variance in arrival energy and the distribution of the matched filtered noise dramatically affects the performance of different active sonar waveforms in time varying shallow water environments. Performance modelling using only the mean signal to noise ratio is not adequate for comparing waveforms because it does not consider these effects.

Acknowledgements

The authors wish to thank Simon Lourey for his advice on statistics and detection systems.

References

[1] Alec Duncan, R. McCauley and A. Maggi, "Predicting the Environmental Impact of Active Sonar", High-Frequency Acoustic Consortium, La Jolla, California 2-10 March 2004

[2] Van Trees H.L., "Optimum signal design and processing for reverberation-limited environment", *IEEE Transactions on Military Electronics* July-Oct 212-229, 1965

[3] Burdic W.S., *Underwater Acoustic System Analysis,* 2nd Edition, Prentice Hall, Englewood Cliffs, New Jersey, 361-379,1991.

[4] Urick R.J., *Principles of Underwater Sound for Engineers,* McGraw-Hill, New York, 304-313, 1967.

[5] Van Trees H.L., *Detection, Estimation, and Modulation Theory Part 3: Radar-Sonar Signal Processing and Gaussian Signals in Noise*, John Wiley and Sons Inc., New York, 316-318, 1971.

[6] Porter M.B., Bucker H.P., "Gaussian beam tracing for computing ocean acoustic fields", *Journal of the Acoustical Society of America*", 82 (4): 1349-1359, 1987

[7] Bucker H.P., "A simple 3 D Gaussian beam sound propagation model for shallow water", *Journal of the Acoustical Society of America"*, 95 (5): 2437-2440, 1994.

[8] Skolnik M.I., *Introduction to Radar systems*, 3rd edition, McGraw-Hill, New York, 295-301, 2001.

[9] Freund J.E., Walpole R.E., *Mathematical statistics,* 4th edition, Prentice-Hill Inc. USA, 299-300, 1987.